Preparation of Nanostrip V 2 O 5 by the Polyol Method and Its Electrochemical Characterization as Cathode Material for Rechargeable Lithium Batteries

ARTICLE *in* THE JOURNAL OF PHYSICAL CHEMISTRY C · SEPTEMBER 2008

Impact Factor: 4.77 · DOI: 10.1021/jp804182z

4 AUTHORS, INCLUDING:

Pitchai Ragupathy
Central Electrochemical Research Institute
24 PUBLICATIONS **547** CITATIONS
SEE PROFILE

Shivakumara Sekharappa
Indian Institute of Science
15 PUBLICATIONS **122** CITATIONS
SEE PROFILE

Vasan H.N.
Indian Institute of Science
24 PUBLICATIONS **608** CITATIONS
SEE PROFILE

Preparation of Nanostrip V_2O_5 by the Polyol Method and Its Electrochemical Characterization as Cathode Material for Rechargeable Lithium Batteries

P. Ragupathy,[†] S. Shivakumara,[†] H. N. Vasan,*[,†] and N. Munichandraiah[‡]

Solid State and Structural Chemistry Unit, Indian Institute of Science, Bangalore-560012, India, and Department of Inorganic and Physical Chemistry, Indian Institute of Science, Bangalore-560012, India

Received: May 12, 2008; Revised Manuscript Received: July 26, 2008

The synthesis of pure nanostrip orthorhombic V_2O_5 was carried out by a simple two-step procedure, with the formation of a vanadyl ethylene glycolate precursor and postcalcination treatment. The precursor and the final product were characterized for its phase and composition by powder X-ray diffraction, infrared spectroscopy, thermal analysis, and X-ray photoelectron spectroscopy. The morphological changes were investigated using field emission scanning electron microscopy and transmission electron microscopy. It was found that the individual strips have around the following dimensions: length, 1.3 μm; width, 332 nm; thickness, 45 nm. The electrochemical lithium intercalation and deintercalation of nanostrip V_2O_5 was investigated by cyclic voltammetry, galvanostatic charge−discharge cycling, galvanostatic intermittent titration technique, and electrochemical impedance spectroscopy. From charge−discharge cycling, the initial discharge capacity of the nanostrip was found to be about 427 mAh g^{-1}. However, it decreased due to inherent phase changes on repeated cycling.

1. Introduction

V_2O_5 is one of the first few cathode materials studied for Li ion batteries.[1−4] It has an orthorhombic layered structure consisting of VO_5 square pyramids sharing edges and corners (Figure 1), and it can intercalate up to 5.4 moles of Li per mole of V_2O_5.[5] Apart from the electrochemically deposited thin films, most of the electrochemical studies carried out in the past were on V_2O_5 particles with size in the range of a few micrometers.[4] With the advent of nanoscience, it is found that the materials of nanosize (<100 nm) have unique electrical, optical, magnetic, catalytic, and thermal properties compared to the bulk.[6−10] V_2O_5 is under reinvestigations in the form of nano structures to improve the intercalation, charge−discharge capacity and cycle life of the Li ion battery.[11] This improvement is mainly due to the manifestation of smaller diffusion length available for the Li^+ ions in the nanosize. To obtain different nanostructures of V_2O_5 various techniques such as thermal evaporation,[12] surfactant assisted solution,[13] hydrothermal/solvothermal,[14] and various other methods have been used. For instance, Pinna et al.[15,16] have prepared γ-V_2O_5 nanorods in reverse micelle emulsions. Nanofibers of V_2O_5 have been synthesized by Livage et al.[17] using a sol−gel technique. Wan et al.[11] have described a polyol process of self-assembled $V_2O_5 \cdot xH_2O$ nanorods into micro spheres. Very recently, Li et al.[18] have obtained V_2O_5 nanowires by hydrothermal synthesis and postcalcination treatment. Some of the interesting studies carried out using such nanostructures include intercalation of Li^+ ions,[11,19] electrochemical super capacitors,[20,21] electrochromic devices,[22,23] catalyst,[24] sensors,[17] etc.

Here, we report the synthesis of high-purity nanostrip V_2O_5 by a simple two-step procedure, which involves preparation of vanadyl ethylene glycolate (VEG) as the precursor, followed by calcination. Both the precursor and the final compound are characterized for chemical composition, phase identification and microscopic structure. Detailed electrochemical characterization studies are performed by cyclic voltammetry, charge−discharge cycling, galvanostatic intermittent titration technique, and alternating current (AC) impedance spectroscopy.

2. Experimental Section

Analytical-grade ammonium metavanadate (NH_4VO_3) and ethylene glycol (EG) were purchased from SD Fine Chemicals Ltd., India and used as such without further purification. $LiAsF_6$, ethylene carbonate (EC), and diethyl carbonate (DEC) were purchased from Sigma-Aldrich, India.

2.1. Synthesis of Nanostrip V_2O_5. NH_4VO_3 (0.01 mol, 1.17 g) was added to 50 mL of EG in a three-necked round-bottom flask. The solution was then refluxed for 2 h at 190 °C while stirring constantly and purging with N_2 gas. At the end of the reaction, a black-colored VEG precipitate was obtained. The precursor product was centrifuged and washed several times with ethanol to remove ethylene glycol and dried in an oven at 50 °C. This was further calcined for 3 h at 600 °C to obtain the final product.

2.2. Characterization. Powder X-ray diffraction (XRD) patterns were recorded for both the precursor and the final product using Cu Kα radiation (λ = 1.5438 Å) in Philips XRD X'PERT PRO diffractometer. To find the chemical composition of the precursor, a detailed thermogravimetric differential thermal analysis (TGA/DTA) were recorded from room temperature up to 600 °C in air using NETZSCH TG 209 F1 thermo gravimetric analyzer. The elemental analysis of carbon and hydrogen were also carried out using a Thermo Finnigan FLASH EA 1112 CHNS analyzer.

IR absorption spectra were recorded in a FT-IR SPECTRUM 1000 PERKIN ELMER spectrometer on thoroughly dried samples using KBr pellets. X-ray photoelectron spectroscopy (XPS) of VEG and V_2O_5 were recorded in an SPECS GmbH spectrometer (Phoibos 100MCD Energy Analyzer) using Al Kα radiation (1486.6 eV). Binding energies were calibrated with respect to C (1s) at 285 eV with a precision of ±0.2 eV. For

* To whom correspondence should be addressed. Phone: +91 80 22933310. Fax: +91-80-23601310. E-mail: vasan@sscu.iisc.ernet.in.
[†] Solid State and Structural Chemistry Unit, Indian Institute of Science.
[‡] Department of Inorganic and Physical Chemistry, Indian Institute of Science.

10.1021/jp804182z CCC: $40.75
Published on Web 09/26/2008

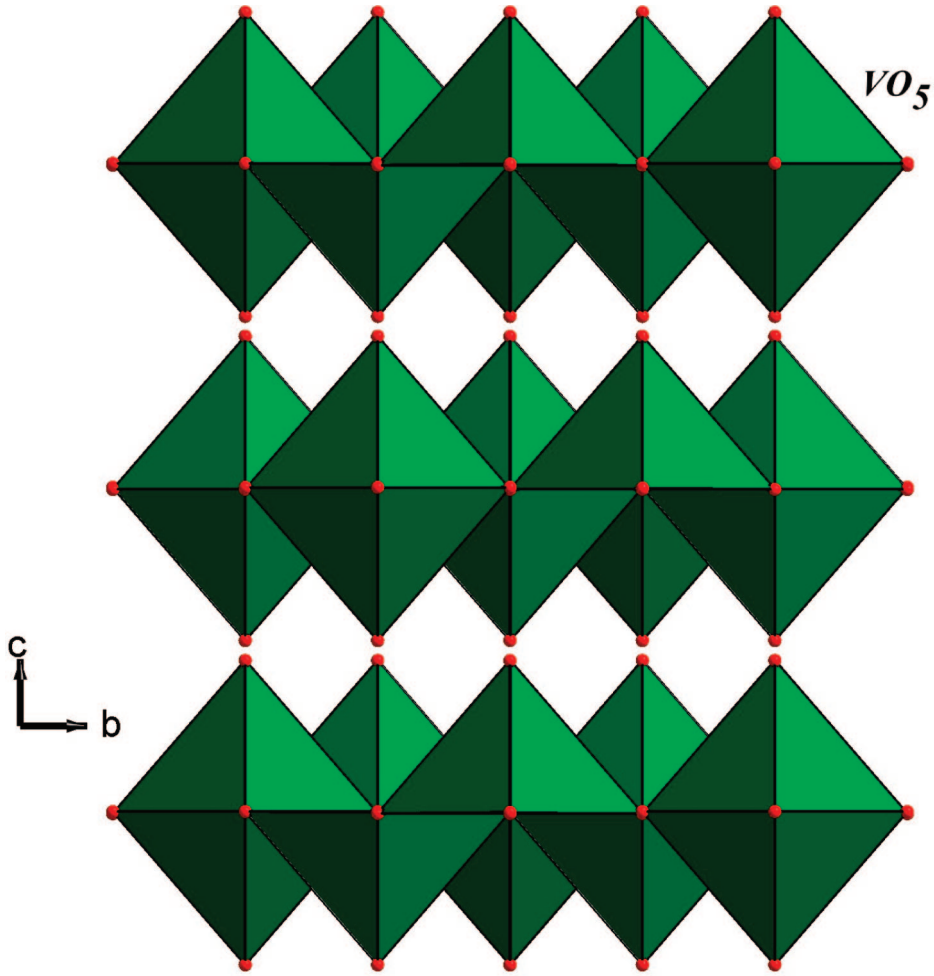

Figure 1. Structure of layered orthorhombic V_2O_5 showing the square pyramids of VO_5 sharing edges and corners.

XPS analysis, the powder samples were pressed into 0.5 mm thick and 8 mm diameter pellets. A pellet was placed inside an ultra high vacuum chamber at 10^{-9} Torr housing the analyzer. Morphological studies were carried out by field emission scanning electron microscopy (FESEM) on Au-coated samples and high resolution transmission electron microscopy (HRTEM) images were obtained by mounting the sample on carbon coated copper grids in Hi Tecnai, operated at 300 kV. Sartorious balance of model CP22D-OCE with 10-μg sensitivity was used for weighing the electrodes and materials.

2.3. Electrode Preparation and Electrochemical Characterization. For electrochemical studies, the electrodes were prepared on an Al foil of thickness 0.2 mm with an area of 1.57 cm^2, which was polished earlier with different grades of emery and cleaned with detergent and washed with double distilled water. A syrup of the electrode material was made by blending 75 wt % of V_2O_5, 20 wt % of acetylene black, and 5 wt % of polyvinylidene fluoride (PVDF) with a few drops of *n*-methyl pyrrolidinone (NMP) applied on to the electrode and dried. Coating and drying steps were repeated three times and finally dried at 110 °C for 12 h in vacuum. The loading level of the active material on the current collector was typically 2.15 mg cm^{-2}. Cells were assembled in an argon-filled M Braun glovebox model Unilab using airtight glass containers. Lithium ribbon (Aldrich) was used as both the counter and reference electrodes. A Celgard microporous polypropylene film (2400) was used as the interelectrode separator. The electrolyte used was 1 M $LiAsF_6$ in EC and DEC mixtures of equal volumes. These mixtures of solvents were treated repeatedly with molecular sieves of grade 4 Å prior to preparation of the electrolyte. Cyclic voltammetry, galvanostatic intermittent titrations, charge−discharge cycling, and electrochemical impedance measurements were performed using Solatron potentiostat model 1286 coupled with frequency response analyzer model 1255B. Impedance data were analyzed using a nonlinear least-squares data fitting program supplied by Solartron with the aid of an electrical equivalent circuit.

3. Result and Discussion

Ethylene glycol (EG) is a well-known solvent used in the preparation of small metal particles, and the preparation procedure is known as the polyol method.[25−27] Ethylene glycol is not only a reducing agent but also a cross-linking reagent.[27,28] It coordinates to the central metal ion to form a metal glycolate further leading to subsequent oligomerization.[28,29] Whittingham et al.[30] have synthesized VEG by a hydrothermal process involving the heat treatment at 200 °C for 2 days by using V_2O_5 and EG. In contrast, we are able to synthesize VEG by refluxing NH_4VO_3 in EG at about 190 °C for 2 h. As the starting compounds and also the reaction conditions influence the chemical composition, morphology, etc. of the product, we have analyzed in detail the precursor by using various analytical techniques.

3.1. XRD Studies. Powder XRD patterns of the precursor and the product obtained by heating the precursor at 600 °C are shown in parts a and b of Figure 2, respectively. XRD pattern of the precursor matches with the reported pattern for VEG

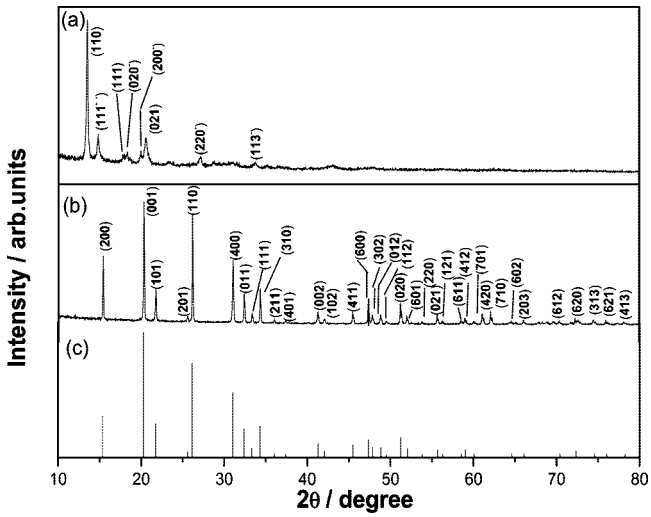

Figure 2. XRD patterns (Cu Kα = 1.5418 Å) of precursor VEG (a), nanostrip V_2O_5 (b), and the JCPDS pattern of orthorhombic V_2O_5 (c). The *hkl* planes are indicated.

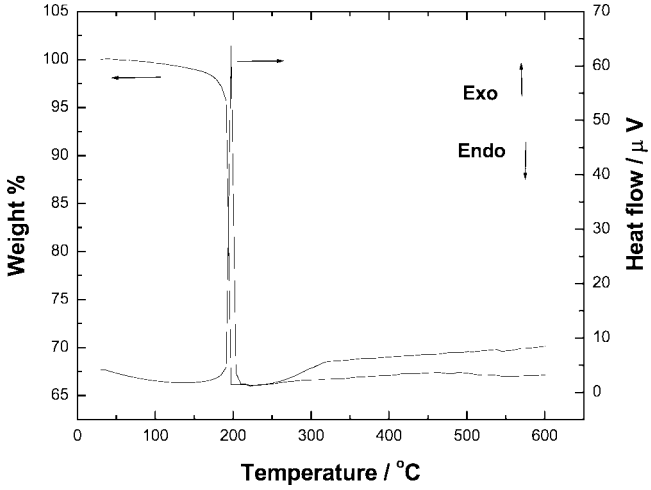

Figure 3. TGA/DTA curves of precursor VEG.

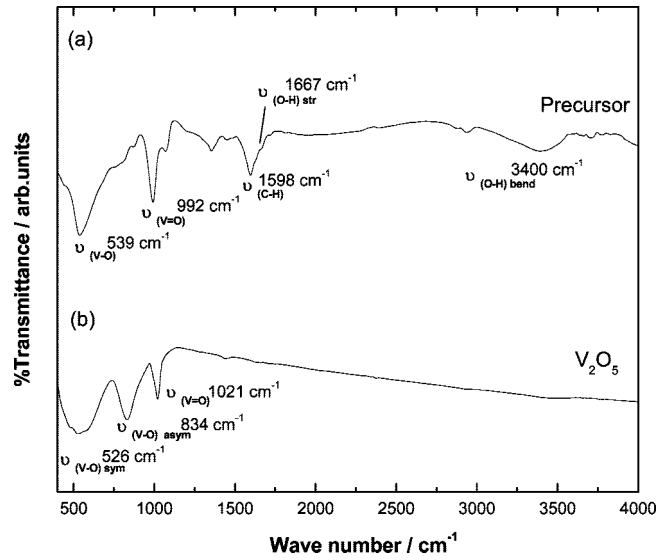

Figure 4. IR spectra of precursor VEG (a) and nanostrip V_2O_5 (b).

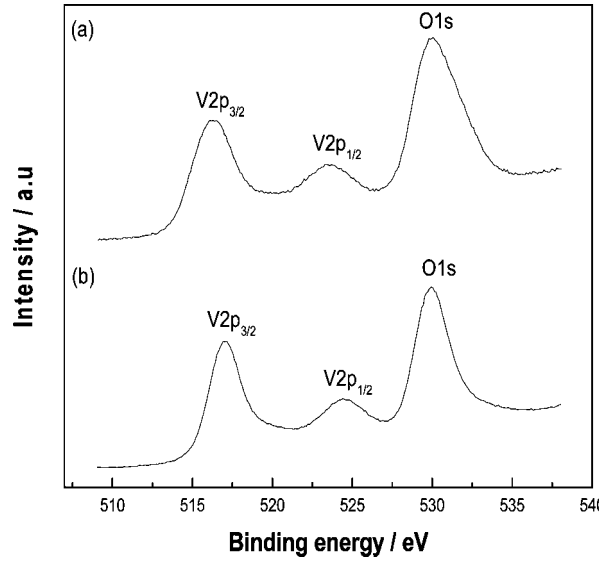

Figure 5. XPS spectra for V $2p_{3/2}$, V $2p_{1/2}$, and O 1s in VEG (a) and nanostrip V_2O_5 (b).

(JCPDS No 49-2497) with space group *C*2/*c* and the calcined product to orthorhombic V_2O_5 (JCPDS No 41-1426) with space group *Pmmn*.

3.2. TGA. Figure 3 shows the TGA/DTA plot recorded in air up to 600 °C. There is a total weight loss of 33.2% (expected loss 34.7%) around 200 °C, corresponding to the decomposition of the VEG to VO_2.[30] This is accompanied by a sharp exothermic peak around 197 °C as seen in Figure 3. On further heating to 600 °C, there is a gain in weight with the total loss of 29.82% (expected loss 28.4%), corresponding to the formation of V_2O_5. This was further confirmed by powder XRD pattern of the sample used for TGA. The carbon and hydrogen analysis also confirms the composition of the VEG.

3.3. Vibrational Spectroscopy Studies. IR spectra of both precursor and orthorhombic V_2O_5 were recorded and shown in Figure 4. The 3400 and 1667 cm^{-1} bands correspond to O−H stretching and bending modes, and the peak at 1598 cm^{-1} corresponds to CH_2O group of glycolate (Figure 4a). The peaks at 992 and 539 cm^{-1} correspond to stretching of V═O and V−O bonds, respectively. Similar spectra were also observed in the earlier studies.[30] In Figure 4b, the peaks at 526 and 834 cm^{-1} correspond to the symmetric and asymmetric stretching of the V−O−V bond, respectively, whereas the peak around 1021 cm^{-1} is assigned to the V═O stretching vibration.[31] The absence of other peaks corresponding to glycolate (Figure 4a), indicates complete decomposition of the VEG.

3.4. XPS Studies. The XPS spectra of the V 2p and O 1s regions of VEG and V_2O_5 are shown in Figure 5 to ascertain the oxidation state of vanadium. The binding energies of V $2p_{3/2}$ and V $2p_{1/2}$ in VEG are found to be 516.22 and 523.48 eV, respectively (Figure 5a). These values are the characteristic for vanadium(IV). After annealing the VEG to 600 °C, it is found that the binding energy is shifted to higher magnitude as shown in Figure 5b (V $2p_{3/2}$, 517.04 eV; V $2p_{1/2}$, 524.47 eV) indicating the formation of V_2O_5 where vanadium exists in +5. The O 1s peak at 529.94 eV is attributed to V−O stretch in both the samples. These values are in agreement with the reported literature.[12,32] From these thermal, elemental, IR, and XPS studies we arrive at the formula $VO(CH_2O)_2$ for the vanadyl ethylene glycolate having the structure.[30]

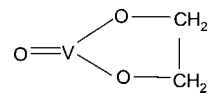

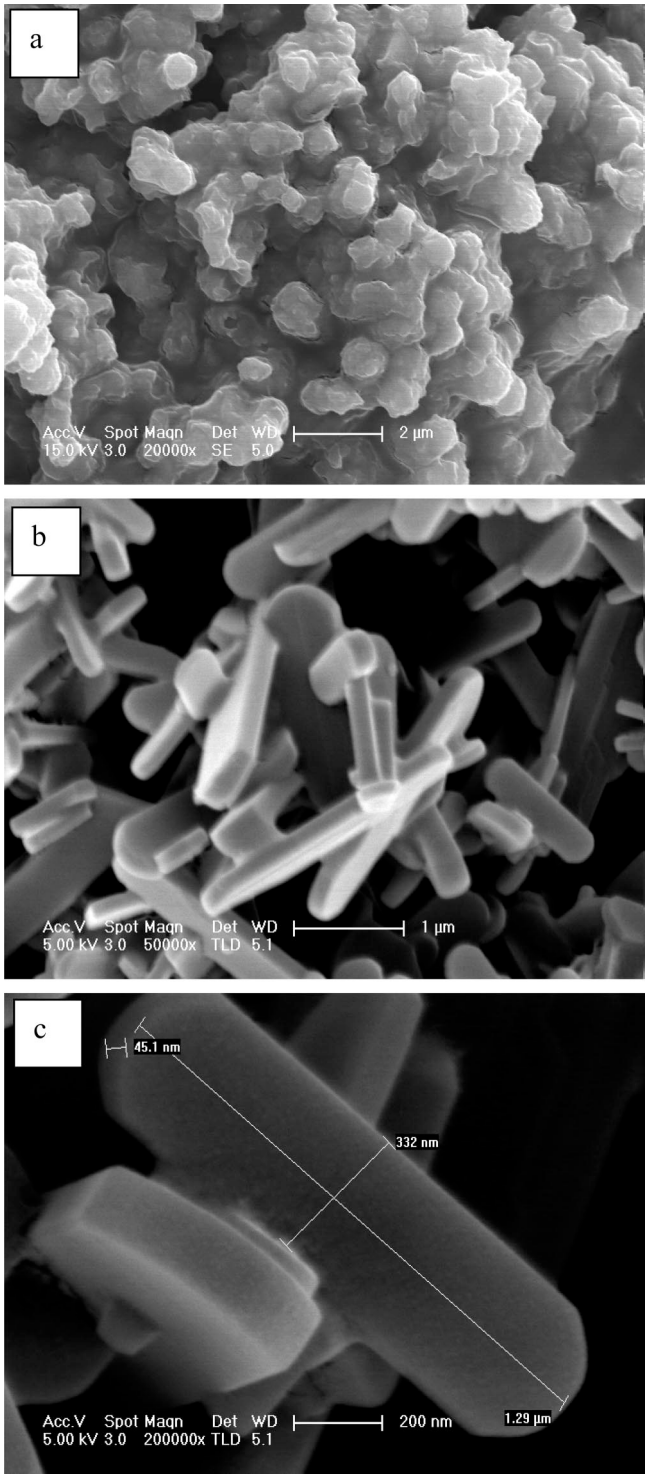

Figure 6. SEM images of precursor VEG (a), nanostrip V_2O_5 (b), and nanostrips at high magnification (c).

3.5. SEM and TEM Studies. SEM images of VEG and orthorhombic V_2O_5 are shown in parts a and b of Figure 6, respectively. The VEG sample does not show any defined morphology, whereas the V_2O_5 exhibits clusters consisting of well-defined strips, with typical dimensions of thickness, 45 nm; width, 332 nm; length, 1.3 μm (Figure 6c).

A typical TEM bright-field image of nanostrip V_2O_5 along with the energy-dispersive X-ray analysis (EDAX) pattern is shown in Figure 7a. The SAED pattern recorded in [001] zone axis indicates the single crystalline nature of the individual strips as shown in Figure 7b. The corresponding diffraction spots

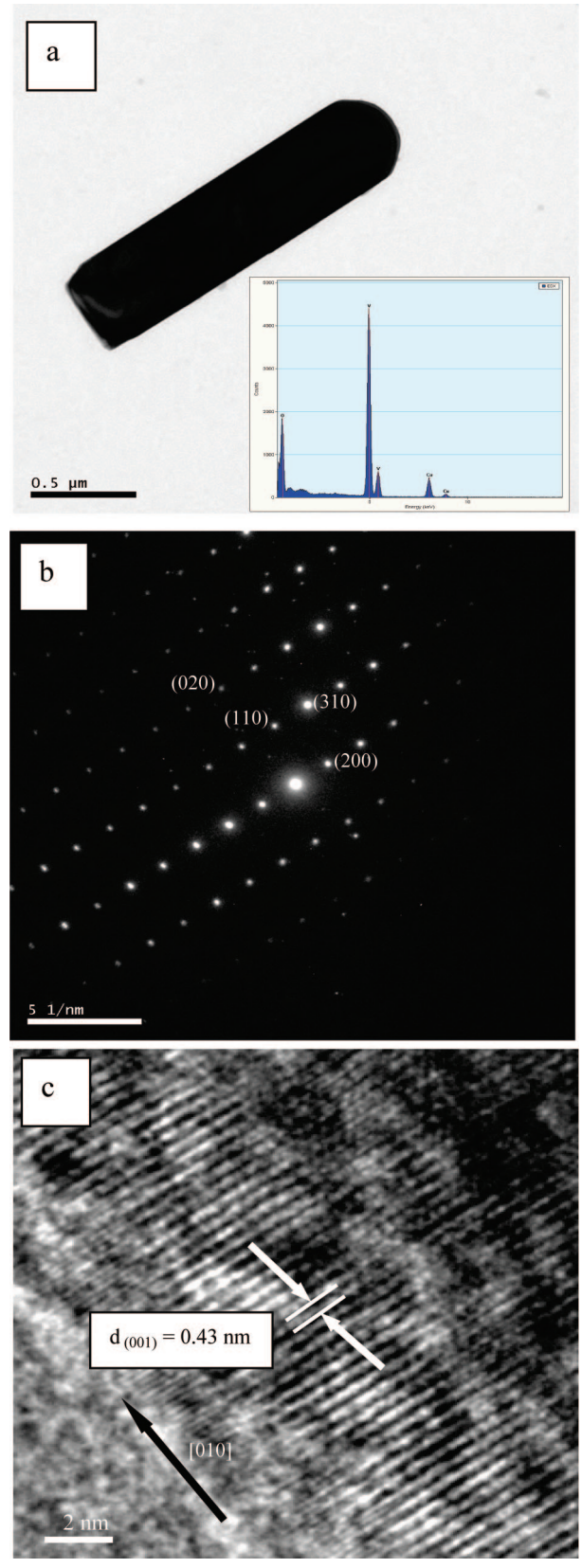

Figure 7. Bright-field TEM image of nanostrip V_2O_5 with EDAX pattern as inset (a), selected area electron diffraction (SAED) pattern of nanostrip V_2O_5 (b) and HRTEM images of the nanostrip (c).

observed in the SAED pattern confirms the orthorhombic form of V_2O_5 crystals. The lattice fringes having inter planar spacing 0.43 nm are seen in HRTEM image (Figure 7c), which correspond to the (001) plane as observed in the XRD pattern

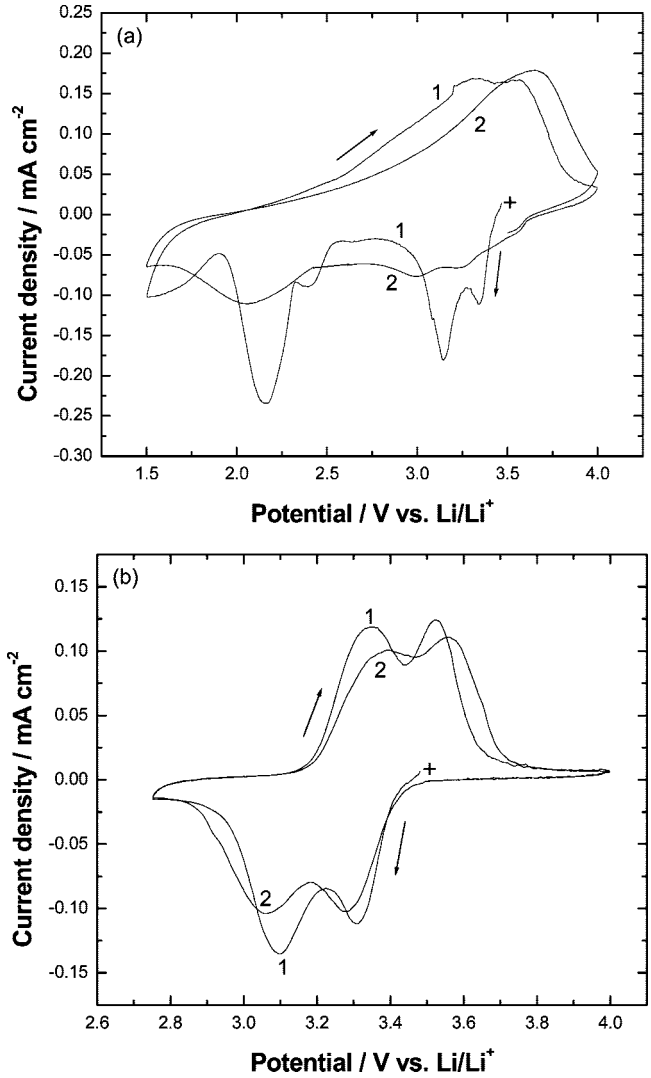

Figure 8. Cyclic voltammograms of nanostrip V_2O_5 recorded in 1 M $LiAsF_6$ electrolyte at sweep rate of 0.075 mV s^{-1} in potential ranges 1.5−4.0 V (a) and 2.75−4.0 V (b). Curves 1 and 2 indicate voltammograms recorded during the first and second cycles, respectively.

(Figure 2b). These observations indicate that the single crystal nanostrips were grown along the [010] direction. Our results are consistent with the earlier report.[33]

3.6. Electrochemical Studies. It is known that V_2O_5 exhibits electrochemical redox behavior, and intercalation and deintercalation of Li^+ occurs during the reversible redox process

$$V_2O_5 + xLi^+ + xe^- \rightleftarrows Li_xV_2O_5 \quad (1)$$

Cyclic voltammograms were recorded to study the electrochemical behavior of nanostrip V_2O_5 (Figure 8a). During the first cycle starting from 3.5 V, four reduction current peaks at 3.34, 3.15, 2.41, and 2.16 V are clearly observed. This suggests that the reduction of V_2O_5 takes place as a multistep process between 1.5 and 3.5 V. In the reverse sweep of the first cycle (curve 1), there are two broad current peaks at 3.31 and 3.56 V. When the electrode was cycled again, the sharp reduction peaks disappear, but broad humps are observed (curve 2, Figure 8a). The oxidation branch of the voltammogram of the second sweep remains nearly the same as that of the first sweep but with a single broad peak at 3.65 V. Similar to the present study, unsymmetrical cathodic and anodic branches of the first voltammogram and fading of current peaks during the subsequent cycling are reported.[5] The four reduction peaks are assigned to successive phase transformations, which accompany the Li^+ insertion process. The phases include α-V_2O_5, ε-$Li_xV_2O_5$, δ- $Li_xV_2O_5$, γ- $Li_xV_2O_5$, and ω-$Li_xV_2O_5$ in series with increasing x value. As the reduction and oxidation branches of the first voltammogram are unsymmetrical, some of the phase transformations are attributed to be irreversible.[5] This irreversible electrochemical behavior of the first voltammogram leads to the appearance of second and subsequent voltammograms without any clear current peaks. Although V_2O_5 prepared in the present study has nano dimension, the electrochemical behavior is similar to the studies already reported for the bulk samples. It is inferred that V_2O_5 undergoes phase transformations during electrochemical cycling, which are inherent to the material irrespective of its particle size and shape.

To examine the influence of potential range on redox behavior of V_2O_5, an electrode was subjected to cyclic voltammetry between 4.0 and 2.75 V, and two repetitive voltammograms are presented in Figure 8b. A pair of cathodic peaks at 3.31 and 3.10 V and the corresponding pair of anodic peaks at 3.34 and 3.52 V are present on the first voltammogram (curve 1, Figure 8b). The voltammogram is nearly reproducible during the second cycle (curve 2, Figure 8b) but with a small decrease in peak current values. These features of voltammetry suggest that V_2O_5 possesses reproducible redox behavior in the potential range 2.75−4.0 V (Figure 8b) better than in the range 1.5−4.0 V (Figure 8a). The cathodic peaks at 3.31 and 3.10 V are attributed to the formation of ε-$Li_xV_2O_5$ and δ-$Li_xV_2O_5$ phases, and the anodic peaks at 3.34 and 3.52 V to oxidation of these two phases back to V_2O_5. As the voltammograms are symmetrical, the electrochemical intercalation/deintercalation of Li^+ ions into/from V_2O_5 is reversible. The electrochemical reversibility leads to the presence of reproducible voltammogram during the second cycle (curve 2, Figure 8b)

Further, the V_2O_5 electrodes were subjected to galvanostatic charge−discharge cycling between 1.5 and 4.0 V. The typical variation of electrode potential during the first cycle is shown in Figure 9a. The discharge proceeds in multiple stages, which are reflected in different potential plateaus, similar to the multiple cathodic peaks present at the first voltammogram of cyclic voltammetry (curve 1, Figure 8a). The overall discharge capacity of 427 mAh g^{-1} is obtained. This value of capacity corresponds to intercalation of Li^+ to the extent of 2.9 moles per mole of V_2O_5. Thus, the formula of the compound in the discharged stage is $Li_{2.9}V_2O_5$. When the electrode is charged up to 4.0 V (Figure 9a), it gains a charge of about 370 mAh g^{-1}, but without any potential plateaus corresponding to the discharge plateaus. The nature of the electrode during charging without plateau is similar to the voltammetric nature from 1.5 to 4.0 V (Figure 8a) where no anodic peaks corresponding to the sharp cathodic peaks are observed. During the subsequent charge−discharge cycling of the electrode, the discharge capacity decreased substantially, and the discharge plateaus disappeared completely. Similar discharge behavior is reported by Delmas et al.[3] During the first discharge of the V_2O_5 electrodes, plateaus I and II (see Figure 9a) occur at a potential range greater than 3.0 V. The amount of intercalated Li till the end of the plateau II corresponds to 0.94 mol per mole V_2O_5, thus forming the phase of composition close to LiV_2O_5. During plateau III, there are some structural reorganizations, and therefore there is a loss of electrochemical reversibility.[3] At the end of plateau IV, Delmas et al.[3] proposed that a new material, ω-$Li_xV_2O_5$ ($x \approx 3$) is irreversibly formed. Although the plateau features are

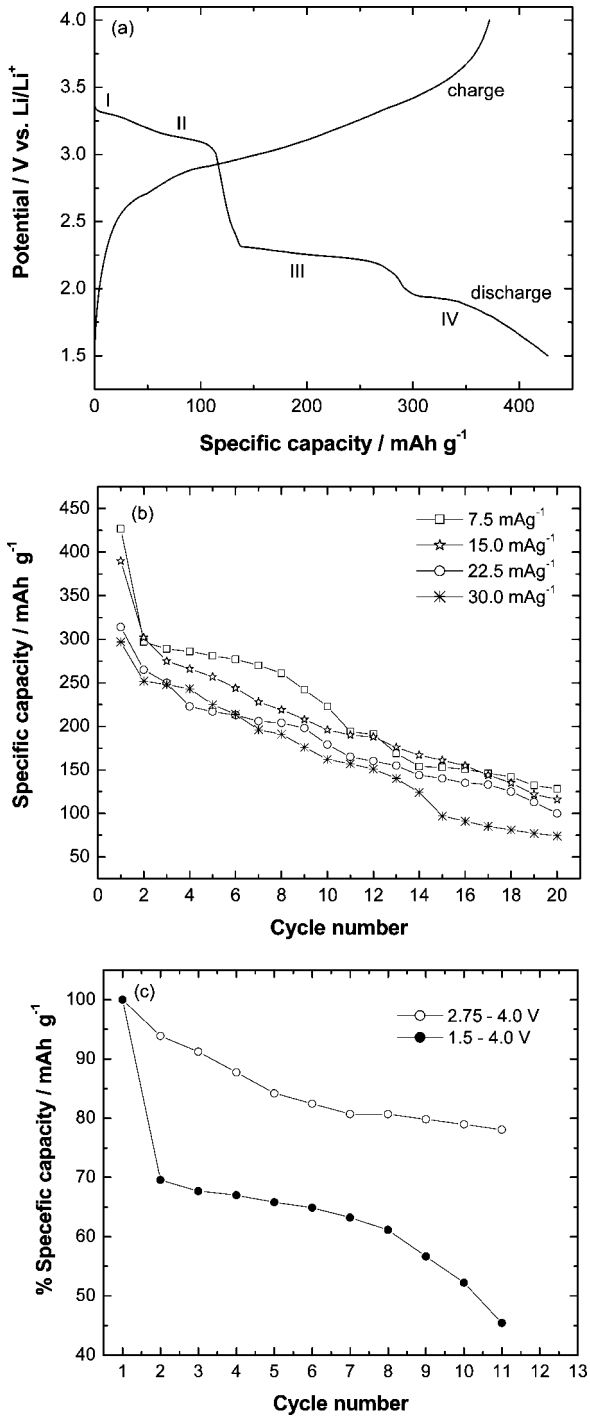

Figure 9. Charge−discharge curves of nanostrip V_2O_5 electrode at current density of 7.5 mA g^{-1} (a), specific capacity at different current densities versus cycle number (b), and percentage of specific capacity loss at two different potential ranges vs cycle number (c).

lost during the first charging and the subsequent charge−discharge cycles, deintercalation of Li from ω-$Li_xV_2O_5$ is shown to occur to a considerable extent. Therefore, V_2O_5 electrodes were subjected to repeated charge−discharge cycling with varied rates. The variation of discharge capacity with cycle number is shown in Figure 9b for several rates of cycling. At the end of the 20th cycle with 7.5 mA g^{-1}, the discharge capacity decreased to about 125 mAh g^{-1} from 427 mAh g^{-1} obtained for the initial discharge. Thus, there is a decrease of about 70% in the discharge capacity during 20 charge−discharge cycles. With an increase of current (Figure 9b), there is a decrease of capacity

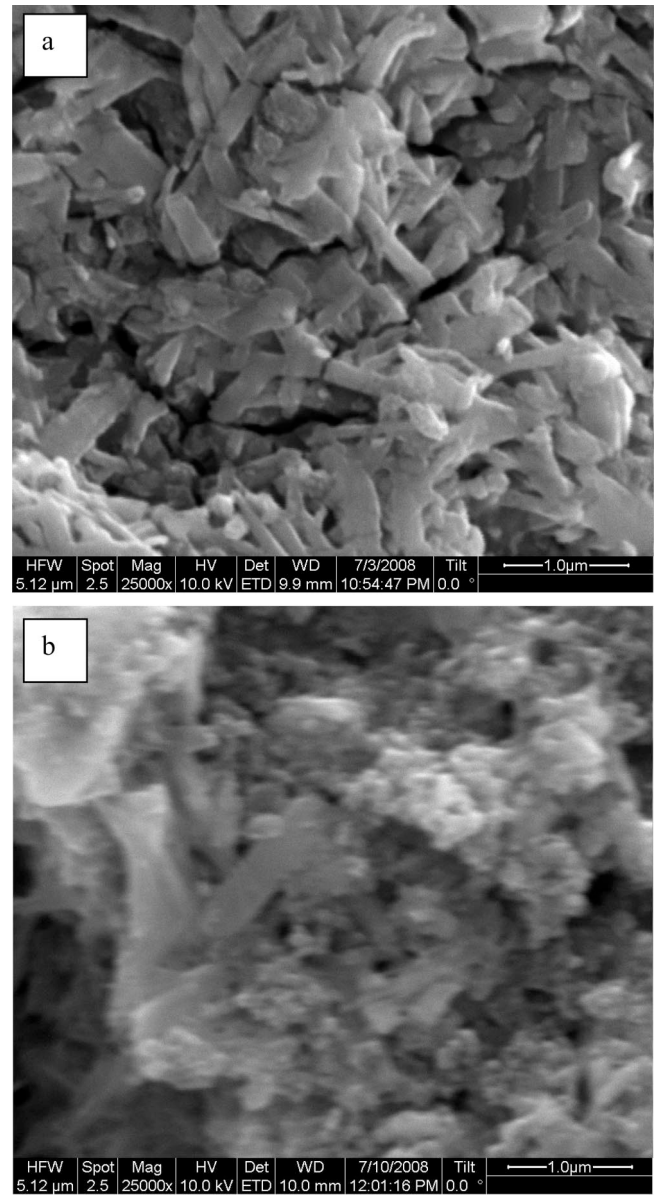

Figure 10. SEM images of V_2O_5 electrode cycled 1 (a) and 20 times (b).

as expected due to decreased utilization of electrode material. The trend of decrease in discharge capacity with cycle number is the same irrespective of the current. Because the V_2O_5 electrodes exhibited better reversible behavior in the potential range 2.75−4.0 V, electrodes were subjected to charge−discharge studies in this potential range also. The discharge capacity obtained was only about 100 mAh g^{-1} in this potential range as expected against a value of 427 mAh g^{-1} obtained in 1.5−4.0 V range (Figure 9a). Nevertheless, the discharge capacity was more stable in 2.75−4.0 V on repeated cycling than at 1.5−4.0 V as shown in Figure 9c. There is 20% decrease in capacity in 2.75−4.0 V during 11 cycles against about a 55% decrease in potential range 1.5−4.0 V.

A V_2O_5 electrode was subjected to a partial discharge to state-of-charge (SOC) of about 0.8, it was allowed to rest for a few hours to reach a steady value of open circuit potential and then subjected to galvanostatic intermittent titration technique (GITT) for measuring solid-state diffusion coefficient of Li^+. A discharge current of 10 μA was injected for about 10000 s, and the electrode potential was measured from its initial value (E_0).

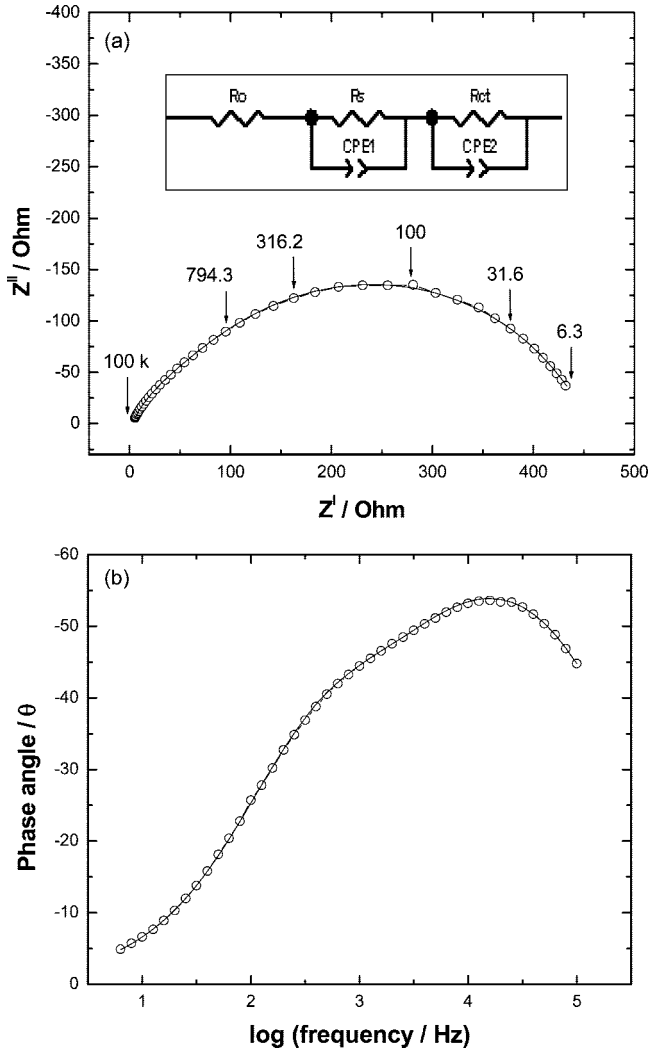

Figure 11. Nyquist plot of the impedance data of nanostrip V_2O_5 electrode with the equivalent circuit as inset, where R_o, R_s, R_{ct}, CPE1, and CPE2 refer ohmic resistance, resistance of surface film, charge-transfer resistance, constant phase element arising from capacitance of surface film and constant phase element arising from double-layer capacitance respectively (frequency values are indicated for some data points in Hz) (a) and Bode phase angle plot of the impedance data (b). Experimental data are presented as open circles and theoretical data as line curves.

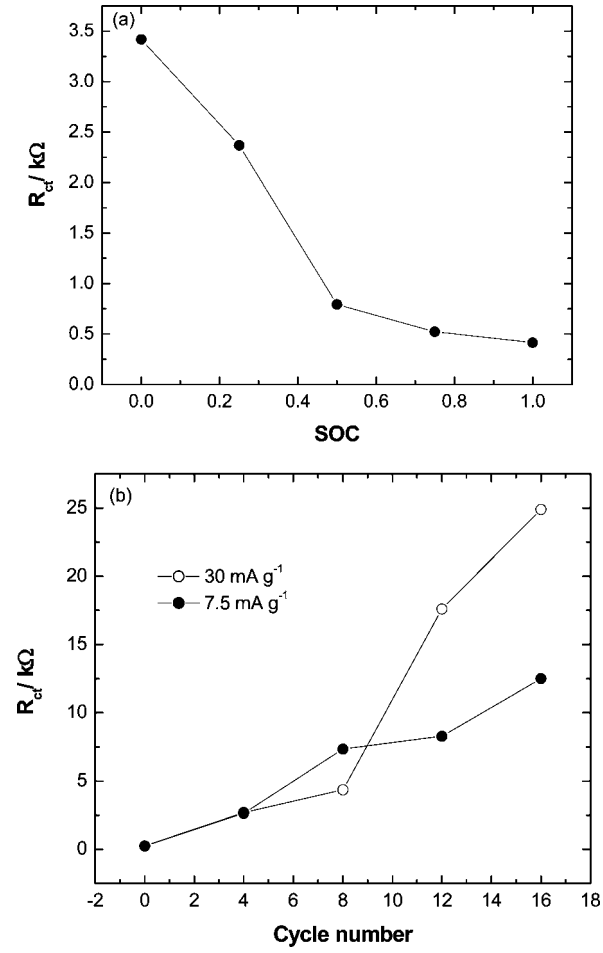

Figure 12. Variations of charge-transfer resistance with SOC of the electrode (a) and with cycle number (b).

Subsequent to reaching of potential to E_t during low discharge, the discharge circuit was disconnected, and potential was measured till it reaches steady value (E_s). Diffusion coefficient (D) was calculated using eq 2.[34,35]

$$D = (4/(\pi\tau))(mV_m/MA)^2(\Delta E_s/\Delta E_\tau)^2 \qquad (2)$$

where m is mass of the active material, M is molar mass, V_m is molar volume, A is area of the electrode, ΔE_s is ($E_o - E_s$), and ΔE_τ is ($E_o - E_\tau$). The apparent value of D obtained was 1.37×10^{-11} cm^2 s^{-1}. A wide range of D values of Li^+ in V_2O_5 are reported in the literature.[36−40] Asai et al.[39] synthesized amorphous V_2O_5, and Li^+ diffusion was measured from a nuclear magnetic response study. They reported a value of 4×10^{-14} cm^2 s^{-1} for D of the Li^+ ion in V_2O_5. Holland et al.[40] synthesized V_2O_5 by two different procedures and reported D of Li^+ by GITT. The calculated values ranged from 5×10^{-8} cm^2 s^{-1} to 1×10^{-13} cm^2 s^{-1}, which depended on the synthetic route and SOC of the electrode. Thus, the value of D measured in the present study for Li^+ ion diffusion in nanostrip V_2O_5 falls within the range of values reported. The nanodimensions of the electrode material may not enhance the diffusion coefficient value, but the diffusion path length is decreased.

It was intended to examine whether or not V_2O_5 retains nanostrip dimensions after the electrodes were cycled. Shown in Figure 10 are SEM micrographs obtained on V_2O_5 electrodes after the 1st and 20th cycles. The electrode, which was cycled once (Figure 10a), is seen retaining the nanostrip morphology of V_2O_5, in spite of the fact that the compound undergoes crystallographic phase changes during the first charge−discharge cycle. On the other hand, the original morphology of V_2O_5 is seen to be destroyed at the end of 20th cycle (Figure 10b). This also may be one of the reasons for the poor capacity retention of the electrode.

The electrochemical behavior of nanostrip V_2O_5 was also studied by electrochemical impedance spectroscopy. Typical impedance data of a V_2O_5 are shown in Figure 11 as Nyquist and Bode plots. There is a high-frequency intercept on the real axis of the Nyquist plot (Figure 11a), which is due to ohmic resistance of the electrochemical cell. The broad semicircle comprises two semicircles, which are overlapped with each other. The presence of two time constants is noticed in the Bode phase angle plot (Figure 11b). The properties of the two semicircles are evaluated by using nonlinear least-squares fitting program and an appropriate equivalent circuit[41] shown as inset in Figure 11a. The high-frequency semicircle is attributed to surface film on the electrode, the low-frequency semicircle to the charge-transfer resistance and double layer capacitance of the electrode. The electrode was subjected to discharge and

impedance was measured at several state-of-charge (SOC) values of the electrode. The charge-transfer resistance (R_{ct}) of the electrode, which is attributed to vanadium redox couple (e.g., V^{5+}/V^{4+}) is presented in Figure 12a as a function of SOC. It is seen that R_{ct} was about 0.5 k Ω at SOC ≈ 1.0, and it increases to about 3.5 k Ω at SOC ≈ 0. The increase in R_{ct} with decreasing SOC is due to decreasing kinetics of redox reaction, which is generally observed for other battery electrode materials.[42,43] Impedance was also measured in the charged state (SOC ≈ 1) for electrodes during repeated charge−discharge cycling. It is seen (Figure 12b) that R_{ct} increases with cycle number, suggesting unfavorable changes taking place in V_2O_5, which are also reflected in charge−discharge cycling studies (Figure 9).

4. Conclusions

Nanostrips of V_2O_5 were prepared via the formation of vanadyl ethylene glycolate in a fast procedure by refluxing NH_4VO_3 and ethylene glycol. V_2O_5 obtained after heating vanadyl ethylene glycolate was characterized by XRD, TGA, IR, XPS, and electron microscopy studies. The electrochemical characterization studies revealed that the nanostrip V_2O_5 was electrochemically active with a high initial capacity. However, its discharge capacity faded on cycling due to inherent phase changes.

Acknowledgment. H.N.V. thanks DST, Government of India for the financial assistance. The authors thank Prof. M. S. Hegde (SSCU) for helpful discussions on XPS and Ms. C. S. Nimisha (Department of Instrumentation) for XPS experiments.

References and Notes

(1) Whittingham, M. S. *J. Electrochem. Soc.* **1976**, *123*, 315.
(2) Dickens, P. G.; French, S. J.; Hight, A. T.; Pye, M. F. *Mater. Res. Bull.* **1979**, *14*, 1295.
(3) Delmas, C.; Brethes, S.; Menetrier, M. *J. Power Sources* **1991**, *34*, 113.
(4) Shimizu, A.; Tsumura, T.; Inagaki, M. *Solid State Ionics* **1993**, *63−65*, 479.
(5) Gao, L.; Wang, X.; Fei, L.; Ji, M.; Zheng, H.; Zhang, H.; Shen, T.; Yang, K. *J. Cryst. Growth* **2005**, *281*, 463.
(6) Bell, A. T. *Science* **2003**, *299*, 1688.
(7) Xia, Y.; Yang, P.; Sun, Y.; Wu, Y.; Mayers, B.; Gates, B.; Yin, Y.; Kim, F.; Yan, H. *Adv. Mater.* **2003**, *15*, 353.
(8) Tarascon, J. M.; Armand, M. *Nature* **2001**, *414*, 359.
(9) Kamat, P. V. *J. Phys. Chem. B* **2002**, *106*, 7729.
(10) Mostafa, A. E-S. *Acc. Chem. Res.* **2001**, *34*, 257.
(11) Cao, A. M.; Hu, J. S.; Liang, H. P.; Wang, L. J. *Angew. Chem., Int. Ed.* **2005**, *44*, 4391.
(12) Lindstrom, R.; Maurice, V.; Groult, H.; Perrigaud, L.; Zanna, S.; Cohen, C.; Marcus, P. *Electrochim. Acta* **2006**, *51*, 5001.
(13) Pavasupree, S.; Suzuki, Y.; Kitiyanan, A.; Pivsa-Art, S.; Yoshikawa, S. *J. Solid State Chem.* **2005**, *178*, 2152.
(14) Liu, J.; Wang, X.; Peng, Q.; Li, Y. *Adv. Mater.* **2005**, *17*, 764.
(15) Pinna, N.; Wild, U.; Urban, J.; Schlogl, R. *Adv. Mater.* **2003**, *15*, 329.
(16) Pinna, N.; Willinger, M.; Weiss, K.; Urban, J.; Schlogl, R. *Nano Lett.* **2003**, *3*, 1131.
(17) Livage, J. *Chem. Mater.* **1991**, *3*, 578.
(18) Li, X.; Li, W.; Ma, H.; Chen, J. *J. Electrochem. Soc.* **2007**, *154*, A39.
(19) Takahashi, K.; Limmer, S. J.; Wang, Y.; Cao, G. Z. *J. Phys. Chem. B* **2004**, *108*, 9795.
(20) Lao, Z. J.; Konstantinov, K.; Tournaire, Y.; Ng, S. H.; Wang, G. X.; Liu, H. K. *J. Power Sources* **2006**, *162*, 1451.
(21) Reddy, R. N.; Reddy, R. G. *J. Power Sources* **2006**, *156*, 700.
(22) Granqvist, C. G. *Handbook of Inorganic Electrochromic Materials*; Elsevier: Amsterdam, 1995.
(23) Ozer, N. *Thin Solid Films* **1997**, *305*, 80.
(24) Ponzi, M.; Duschatzky, C.; Carrascull, A.; Ponzi, E. *Appl. Catal., A* **1998**, *169*, 373.
(25) Fievet, F.; Lagier, J. P.; Figlarz, M. *MRS Bull.* **1989**, *14*, 29.
(26) Feldmann, C. *Adv. Funct. Mater.* **2003**, *13*, 101.
(27) Feldmann, C.; Jungk, H.-O. *Angew. Chem., Int. Ed.* **2001**, *40*, 359.
(28) Jiang, X.; Wang, Y.; Herricks, T.; Xia, Y. *J. Mater. Chem.* **2004**, *14*, 695.
(29) Wang, Y.; Jiang, X.; Xia, Y. *J. Am. Chem. Soc.* **2003**, *125*, 16176.
(30) Weeks, C.; Song, Y.; Suzuki, M.; Chernova, N. A.; Zavalij, P. Y.; Wittingham, M. S. *J. Mater. Chem.* **2003**, *13*, 1420.
(31) Subba Reddy, C. V.; Wei, J.; Yao, Z. Q.; Rong, D. Z.; Wen, C.; Mho, S.; Kalluru, R. R. *J. Power Sources* **2007**, *166*, 244.
(32) Boughriet, A.; Mouchel, B.; Revel, B.; Gengembre, L.; Laureyns, J. *Phys. Chem. Chem. Phys.* **1999**, *1*, 4051.
(33) Chan, C. K.; Peng, H.; Twesten, R. D.; Jarausch, K.; Zhang, X. F.; Cui, Y. *Nano Lett.* **2007**, *7*, 490.
(34) Weppner, W.; Huggins, R. A. *J. Electrochem. Soc.* **1977**, *124*, 1569.
(35) Suresh, P.; Shukla, A. K.; Munichandraiah, N. *J. Electrochem. Soc.* **2005**, *152*, A2273.
(36) Lantelme, F.; Mantoux, A.; Groult, H.; Lincot, D. *J. Electrochem. Soc.* **2003**, *150*, A1202.
(37) Bay, N. T. B.; Tien, P. M.; Badilescu, S.; Djaoued, Y.; Bader, G.; Girouard, F. E.; Truong, V.; Nguyen, L. *J. Appl. Phys.* **1996**, *80*, 7041.
(38) Navone, C.; Hadjean, R. B.; Pereira-Ramos, J. P.; Salot, R. *Electrochim. Acta* **2008**, *53*, 3329.
(39) Asai, T.; Sugimoto, S.; Kawai, S. *Mater. Res. Bull.* **1989**, *24*, 75.
(40) Holland, G. P.; Huguenin, F.; Torresi, R. M.; Buttry, D. A. *J. Electrochem. Soc.* **2003**, *150*, A721.
(41) Boukamp, B. A. *Equivalent Circuit, Users Manual*; University of Twente: The Netherlands, 1989; p 1.
(42) Rodrigues, S.; Munichandraiah, N.; Shukla, A. K. *J. Solid State Electrochem.* **1999**, *3*, 397.
(43) Suresh, P.; Shukla, A. K.; Munichandraiah, N. *J. Appl. Electrochem.* **2002**, *32*, 267.

JP804182Z